International Journal of Solids and Structures 49 (2012) 2962–2977

Contents lists available at SciVerse ScienceDirect

International Journal of Solids and Structures

journal homepage: www.elsevier.com/locate/ijsolstr

Indentation of an elastic layer by a rigid cylinder

J.A. Greenwood [a,*], J.R. Barber [b]

[a] University Engineering Department, Cambridge, UK
[b] Department of Mechanical Engineering, University of Michigan, USA

ARTICLE INFO

Article history:
Received 6 October 2011
Received in revised form 27 March 2012
Available online 12 June 2012

Keywords:
Green's function
Indentation
Elastic layer

ABSTRACT

The Green's functions for the indentation of an elastic layer resting on or bonded to a rigid base by a line load are found efficiently and accurately by a combination of contour integration with a series expansion for small arguments. From the form of the equations it is clear that the function is oscillatory when the layer is free to slip over the base, but for the bonded layer, the function simply decays to zero after a single overshoot.

The deformation due to pressure distributions of the form of the product of a polynomial with an elliptical ("Hertzian") term is calculated and the coefficients chosen to match the indentation shape to that of a cylindrical indenter. The resulting pressure distributions behave much as in Johnson's approximate theory, becoming parabolic instead of elliptical as the ratio b/d of contact width to layer thickness increases, or, for the *bonded incompressible* ($\nu = 1/2$) layer, becoming bell-shaped for very large b/d.

The relation between the approach δ and the contact width b curves has been investigated, and some anomalies in published asymptotic equations noted and, perhaps, resolved.

A noticeable feature of our method is that, unlike previous solutions in which the full mixed boundary value problem (given indenter shape / stress-free boundary) has been solved, the bonded incompressible solid causes no problems and is handled just as for lower values of Poisson's ratio.

1. Introduction

The indentation of a layer by a rigid circular cylinder is of some technological importance, as is evidenced by the origins of the early papers: Hannah (1951) in the Department of Textile Industries (University of Leeds), Miller (1966) from the Printing, Packaging and Allied Trades Research Association. Sadly, neither Meijers (1968) nor, particularly Aleksandrov's contributions (e.g. Aleksandrov (1969)) are easy for an engineer to understand: a situation perhaps explained by Alblas and Kuiper's comment (1970). "We find it difficult to trace the effects [of the two approximations] separately and do not see beforehand whether the two approximations are compatible". Here a relatively simple-minded approach is adopted: we avoid the mixed boundary value problem by finding the solution for a point load (the Green's function) and use this to obtain the indentation shape for a pressure distribution $p = \sqrt{1-t^2}\sum(e_n t^{2n})$ where $t = x/b$ and b is the half-width of the contact. The coefficients e_n are then chosen to approximate the desired indentation shape. The resulting fits appear to be excellent.

The elegant feature of this analysis is the use of contour integration to evaluate the integral for the Green's function, as introduced by Dougall (1904) but rejected by later authors (e.g. Sneddon, 1946) because of the difficulty at the time in performing complex arithmetic. This is no longer a problem: and in practice over much of the range needed it is found that the Green's function is in effect only a single damped exponential term.

2. Green's function for an elastic layer resting on a rigid base

We consider first a layer resting on a rigid, frictionless base, i.e. with no normal displacement or shear stress at its base. A line load $p(x) = \delta(x)$ can be represented by its Fourier integral $p(x) = \frac{1}{\pi}\int_0^\infty \cos(kx)dk$. For a layer of thickness d with no displacement or shear stress at its base (or a symmetrically loaded layer of thickness $2d$), the surface displacement due to $p_1\cos(kx)$ is.

$E'w(x) = \dfrac{2p_1}{k}\dfrac{\sinh^2(\alpha)}{\sinh(\alpha)\cosh(\alpha)+\alpha}\cos(kx)$ where $\alpha = kd$ and E' is the plane strain modulus $E/(1-\nu^2)$. Hence, the displacement $w(x)$ due to a unit line load at $x = 0$ is $w(x) = Y(\xi)/E'$, where $\xi = x/d$ and

$$Y(\xi) = \frac{2}{\pi}\int_0^\infty \frac{\sinh^2(\alpha)}{\sinh(\alpha)\cosh(\alpha)+\alpha}\cos(\alpha\xi)\frac{d\alpha}{\alpha} \tag{1}$$

[Hannah (1951): see also Johnson, 1985 Eq. 5.65, but beware of the one-sided Fourier transform (Eq. 5.66)].

* Corresponding author.
E-mail address: jag@eng.cam.ac.uk (J.A. Greenwood).

0020-7683/$ - see front matter © 2012 Elsevier Ltd. All rights reserved.
http://dx.doi.org/10.1016/j.ijsolstr.2012.05.036

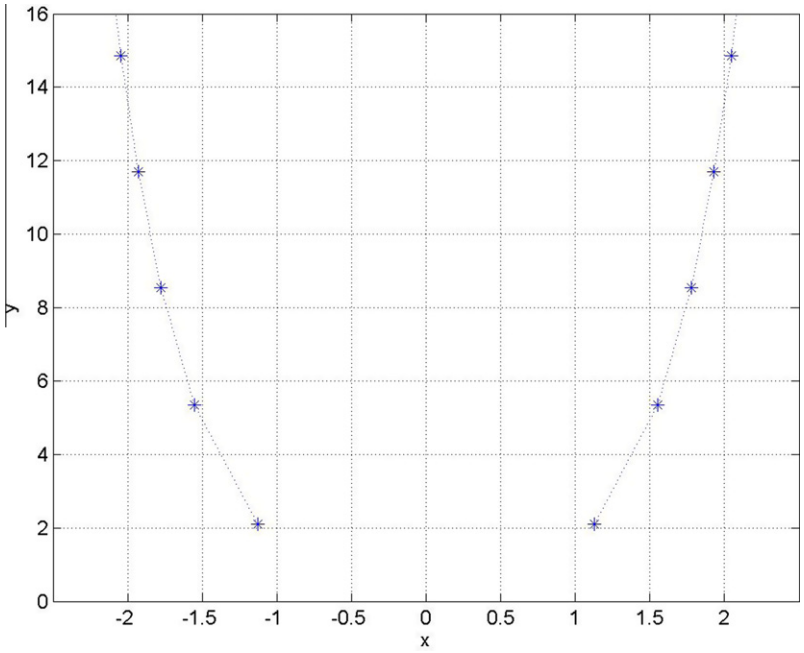

Fig. 1. Poles of $f(z)$ in upper half-plane (unbonded layer).

2.1. Evaluation of $Y(\xi)$ by contour integration

Dougall (1904) introduced the evaluation by contour integration of the related integrals for the axisymmetric loading of a layer, and in this way obtained the leading features of the behaviour. Sneddon (1946), daunted by the complex arithmetic involved, preferred straightforward numerical integration: but now that computer procedures for complex arithmetic are readily available, the scales are tilted the other way. In particular, for large values of ξ, where numerical integration in effect leads to the summation of an alternating series (integrals over the separate loops of $\cos(\xi x)$), with relatively large terms apparently summing to almost zero, the contour integration method is ideal.

Thus, to evaluate $Y(\xi)=\dfrac{2}{\pi}\displaystyle\int_0^\infty \frac{\sinh^2(\alpha)}{\sinh(\alpha)\cosh(\alpha)+\alpha}\cos(\xi\alpha)\frac{d\alpha}{\alpha}$ we consider $\frac{2}{\pi}\oint f(z)\exp(i\xi z)dz$, where $f(z)\equiv\dfrac{\sinh^2(z)}{\sinh(z)\cosh(z)+z}\cdot\dfrac{1}{z}$, along AB, the real axis from $-L$ to $+L$, and returning around the semicircle of radius L. [Note that the function is finite at the origin: $f(0)=1/2$].

Along AB we have $\int_{-L}^{0} f(x)\exp(i\xi x)dx=\int_0^L f(x)\exp(-i\xi x)dx$ since $f(x)$ is even, so that $\int_{AB} f(z)\exp(i\xi z)dz=2\int_0^L f(x)\cos(\xi x)dx$, which letting $L\to\infty$ equals $\pi Y(\xi)$. Thus the value of $Y(\xi)$ can be found from the sum of the residues at the poles $z=z_k$, provided we can establish that the integral round the semicircle vanishes.

2.1.1. Integral round the semicircle

The distance from the kth pole to the origin is approximately $(k-1/4)\pi$, so we take the radius of the semicircle to be $L=n\pi$ to avoid the poles. It is readily found numerically that along the contour $z=n\pi\exp(i\theta)$ $(0\leqslant\theta\leqslant\pi)$ the maximum value of $\left|\frac{\sinh^2(z)}{\sinh(z)\cosh(z)+z}\right|$ is approximately $1+\frac{0.264}{n+1/2}$: more importantly, it is bounded, so that when the factor $1/z$ is included, the function $|f(z)|$ tends uniformly to zero (through integer values of n), and so satisfies the conditions of Jordan's Lemma, establishing that as $n\to\infty$ the integral round the semicircle vanishes.[1]

[1] Dougall (1904) chooses as his contour the square with vertices $\pm n\pi$, $\pm n\pi+2n\pi i$.

2.1.2. Poles and residues

Within the contour the function has simple poles at the zeros of $\{\sinh(z)\cosh(z)+z\}$. (Note that $z=0$ is not a pole: $f(0)=1/2$). Denoting these by $z=z_k$, then $\sinh(z_k)\cosh(z_k)+z_k\equiv(1/2)(\sinh(2z_k)+2z_k)=0$, which is readily solved (using MATLAB) by iteration starting from $2y=(2k-0.6)\pi$; $2x=\ln\{(4k-1)\pi\}$.

Note that there are zeros $(\pm a\pm ib)$ in all four quadrants: only the pairs $(\pm a+ib)$ are relevant. See Fig. 1.

Dougall (1904) gives the asymptotic approximation $2z_k=\ln((4k-1)\pi)+i(4k-1)(\pi/2)$. Accurate values are given in Table 1.

At $z=z_k+t$, the vanishing factor $g(z)\equiv(1/2)(\sinh(2z)+2z)$ becomes approximately $g(z_k+t)\sim tg'(z_k)=t\{\cosh(2z_k)+1\}$ so the residue at $z=z_k$ is $\frac{\sinh^2(z_k)}{z_k\{\cosh(2z_k)+1\}}\exp(i\xi z_k)$, which can conveniently be written $(A_k+iB_k)\exp(i\xi z_k)$.

2.1.3. Paired residues

If the residue at $z=z_k$ is $(A_k+iB_k)\exp(i\xi z_k)$.

Table 1
Data for computing Green's function for the unbonded layer values of $Y(\xi)$ accurate to 10^{-5} can be found as follows.

For $0\leqslant\xi\leqslant 0.4$, *write* $Y(\xi)=-\frac{2}{\pi}\ln\xi+Y_m(\xi)$ *with* $Y_m(\xi)=\sum_{n=0}^{5}a_n\xi^{2n}$.						
n	0	1	2	3	4	5
a_{2n}	−0.223884	0.33170	−0.08591	0.02201	−0.00550	0.00136

For $\xi\geqslant 0.4, Y(\xi)=-4\sum_{k=1}^{8}\exp(-\xi y_k)[A_k\cos(\xi x_k)+B_k\sin(\xi x_k)]$	
Poles $z_k\equiv x_k+iy_k$	Residue factors A_k+iB_k[a]
1.12536 + 2.10620i	0.03091 − 0.25397i
1.55157 + 5.35627i	0.01031 − 0.09370i
1.77554 + 8.53668i	0.00544 − 0.05845i
1.92940 + 11.6992i	0.00343 − 0.04261i
2.04685 + 14.8541i	0.00238 − 0.03357i
2.14189 + 18.0049i	0.00177 − 0.02770i
2.22172 + 21.1534i	0.00137 − 0.02358i
2.29055 + 24.3003i	0.00109 − 0.02053i

[a] The residues are $(A_k+iB_k)\exp(i\xi z_k)$.

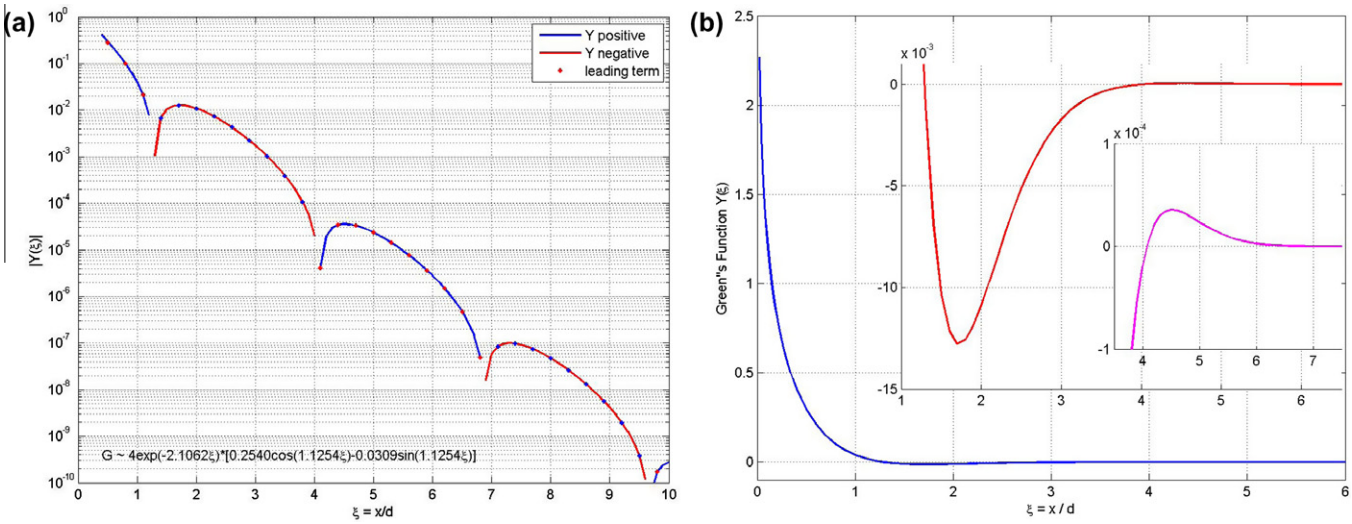

Fig. 2. (a) Green's function, showing mildly oscillatory behaviour at large ξ. (b) Green's function showing oscillatory behaviour in detail. The spots are the values using only the contribution from the first pair of poles.

Since the residue at $z = z_k$ is $(A_k + iB_k)\exp(i\xi z_k)$, the residue at the matching pole $z = -\bar{z}_k$ will be $-(A_k + iB_k)\exp(i\xi\bar{z}_k)$, so that for $\xi = 0$ the sum of the two residues is $2i\,B_k$. For $\xi \neq 0$, the residues are $(A_k + i\,B_k)\exp(-\xi y_k)(\cos(\xi x_k) + i\sin(\xi x_k))$ and $(-A_k + i\,B_k)\exp(-\xi y_k)(\cos(\xi x_k) - i\sin(\xi x_k))$, so adding gives $2i\exp(-\xi y_k)(A_k\sin\xi x_k + B_k\cos(\xi x_k) \equiv 2i\,Imag[f(z_k)\exp(i\xi z_k)]$.

Multiplying the sum of the residues by $2\pi i$ gives $\pi Y(\xi)$.

The results agree beautifully with values previously found by a numerical integration, but now establish clearly the behaviour of the Green's function at large ξ. The results are shown in Fig. 2a, and exhibit a mildly oscillatory behaviour at large ξ shown in the two insets. The leading term is that due to the residues at the first pair of poles $z = (\pm x_1 + i\,y_1)$ giving the asymptotic result

$$Y(\xi) \sim 4\exp(-2.1062\xi)[0.2540\cos(1.1254\xi) - 0.0309\sin(1.1254\xi)].$$

As Fig. 2b shows, this is already a good approximation when $\xi = 1$.

The evaluation of $Y(\xi)$ as the sum of the residues requires more and more terms as ξ decreases, reflecting the fact that the Green's function $Y(\xi)$ will be logarithmically singular near the point of application of the force $x = 0$. This behaviour is determined by the behaviour of the integrand at large α, where $\frac{\sinh^2(\alpha)}{\sinh(\alpha)\cosh(\alpha)+\alpha} \sim \tanh(\alpha)$. In order to extract the singular term analytically, we therefore write $f(\alpha) \equiv \frac{\sinh^2(\alpha)}{\sinh(\alpha)\cosh(\alpha)+\alpha} = f_1(\alpha) - f_2(\alpha)$ where $f_1(\alpha) = \tanh(\alpha)$ and $f_2(\alpha) = \tanh(\alpha) - f(\alpha) = \frac{\alpha\tanh(\alpha)}{\sinh(\alpha)\cosh(\alpha)+\alpha}$.

Now using Gradstein and Rhyzik 4.114.2 we have

$$\int_0^\infty \tanh(\alpha)\cos(\alpha\xi)\frac{d\alpha}{\alpha} = \frac{1}{2}\ln\left\{\frac{\cosh(\pi\xi/2)+1}{\cosh(\pi\xi/2)-1}\right\} = \ln\{\coth(\pi\xi/4)\}$$

and hence we can write $Y(\xi) = Y_1(\xi) - Y_2(\xi)$ with $Y_1(\xi) = -\frac{2}{\pi}\ln\{\tanh(\pi\xi/4)\}$ and the residual term

$$Y_2(\xi) = \frac{2}{\pi}\int_0^\infty f_2(\alpha)\cos(\alpha\xi)\frac{d\alpha}{\alpha} = \frac{2}{\pi}\int_0^\infty \frac{\tanh(\alpha)}{\sinh(\alpha)\cosh(\alpha)+\alpha}\cos(\alpha\xi)\,d\alpha \quad (3)$$

is bounded for all ξ

Since the series for cos$u$ is uniformly convergent, we can expand the cosine in series and integrate term by term: this is convenient for small values of ξ ($\xi \leqslant 0.5$). [Over a substantial range both methods give the same answers (agreeing to 10^{-5}): cf Fig. 9 below for the bonded layer].

2.2. Green's function over the whole range

The contour integration equations were used to give values of the Green's function for $\xi \geqslant 0.4$. The series expansion was used to give values of $Y(\xi) + \frac{2}{\pi}\ln\{\tanh(\pi\xi/4)\}$ for $\xi < 0.4$. [The change-over point is largely arbitrary because of the extensive overlap range]. For further work it was convenient to introduce an auxiliary function $Y_m(\xi) \equiv Y(\xi) + \frac{2}{\pi}\ln(\xi)$ shown in Fig. 3. This is bounded at $\xi = 0$ and convenient for numerical work while the logarithmic term can be treated analytically (see Appendix C). Table 1 gives the coefficients needed to determine the Green's function $Y(\xi)$ over the entire range.

3. Pressure distribution under a roller

It is generally accepted in roller bearing calculations that the Hertzian pressure distribution, $p = (E^*/2R)\sqrt{b^2 - x^2}$, exact for contact between a rigid parabolic indenter and an elastic half-space, is a good approximation to the pressure between a roller and a finite layer (Johnson, 1985). Johnson however assumes the layer thickness d (or more precisely the ratio d/b) to be large. When d/b is not large, it is clear that a pressure distribution consisting of a product of a power series with the Hertzian pressure is likely to be better: so we need to calculate the indentation shape for pressures of this form.

The displacements $w(x)$ will be

$$E'w(x) = \int_{-b}^{+b} p(x')Y(|x - x'|/d)dx' = b\int_{-1}^{+1} p(t')Y\{(b/d)|t - t'|\}dt' \quad (4)$$

As noted above, the logarithmic singularity in the function $Y(\xi)$ is extracted by writing $Y(\xi) \equiv Y_m(\xi) - \frac{2}{\pi}\ln(\xi)$.

3.1. Integration to find the shape

If the pressures $p(x) = \sqrt{1 - x^2/b^2}\sum e_n x^{2n}$ are written in the Chebyshev form $p(\cos\theta) = \sin\theta\sum c_n\cos 2n\theta$ where $t \equiv x/b = \cos\theta$, the integration of the singular term may be done analytically

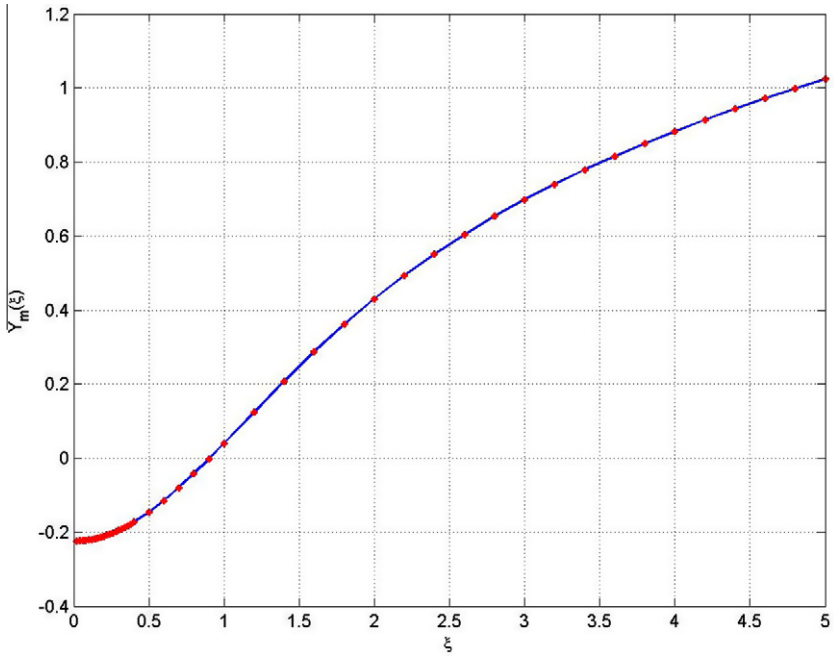

Fig. 3. Non-singular part of the Green's function for a layer of thickness d. To obtain the Green's function $Y(x/d)$ a term $(2/\pi)$ ln (x/d) must be subtracted.

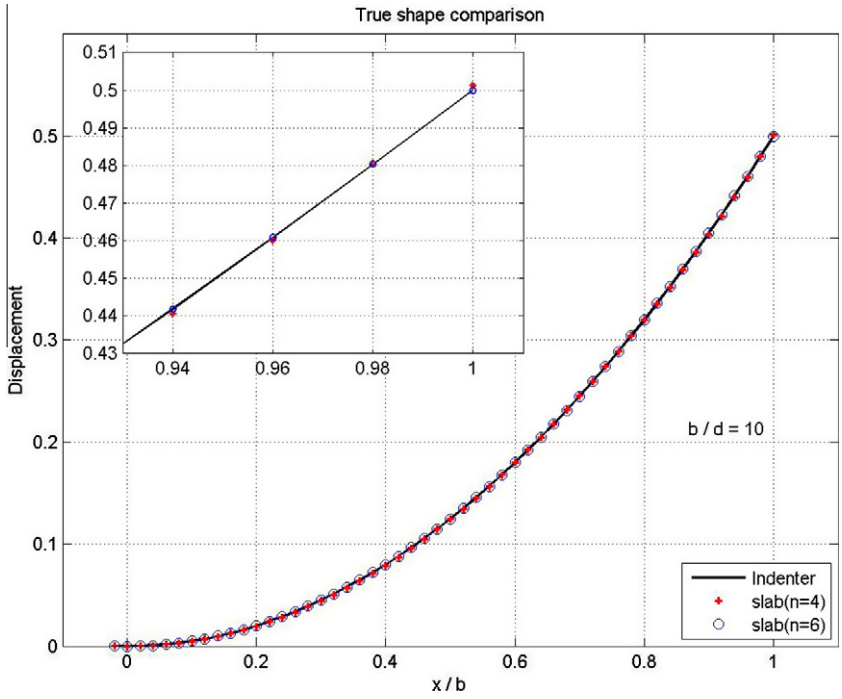

Fig. 4. Matching of shapes of surface and indenter. The shape found is very close to the cylindrical shape desired. Additional terms have little effect.

(see Appendix C) and leads to displacements within the indentation of the form $w(x/b) = \sum C_m \cos(2m\phi)$ where $x = b\cos\phi$.

These can easily converted into a power series in x^2.

The non-singular part of the Green's function, $Y_m(\xi)$ is readily integrated numerically.

The shape coefficients $c_0, c_2, \ldots$ are now chosen to give a shape approximating the indenter shape. The shapes due to the individual pressure terms were curve-fitted to polynomials in x^2 (of order 6) and the coefficients $c_0, c_2, \ldots$ chosen to eliminate the terms in $x^4, x^6 \ldots x^{12}$ and leave just $z = x^2/2$ with excellent results: Fig. 3 shows the fit for an extreme case, $b/d = 10$ and Fig. 4 shows the corresponding pressure distribution. [The inclusion of terms $T_8, T_{10}, \ldots$ improves the fit near $x = b$ but otherwise has little effect].

The calculated pressure distributions are close to the elliptical 'Hertzian' pressures for $b/d \leqslant 1$ (*very* close for $b/d < 0.5$), but approach the parabolic shape predicted by Johnson (1985) for b/d large. The maximum pressure agrees with his prediction that asymptotically

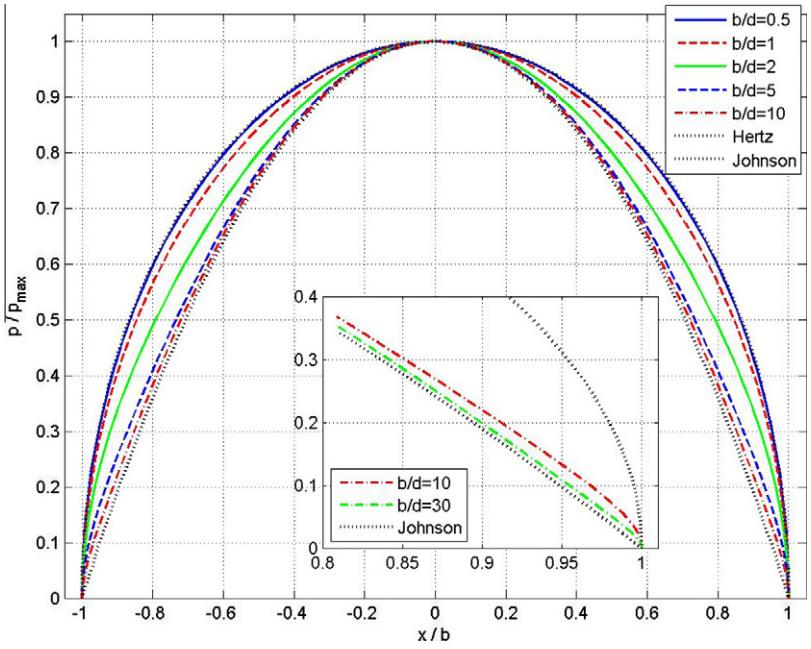

Fig. 5. Development of pressure distribution as b/d increases.

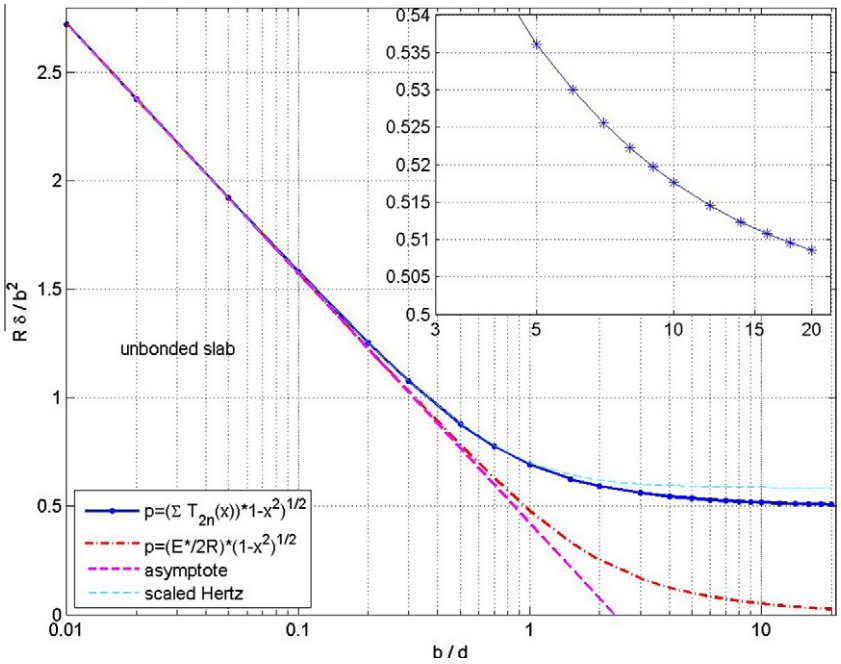

Fig. 6. Displacement for an unbonded layer of thickness d. Note that for b/d small, the result may be written $R\delta = 0.5b^2[\ln(2.320d/b)]$.

$Rp_{max}/E'b \sim b/2d$ but with a small offset $[b/2d + 0.183]$ (see Fig. 16 below).

3.2. Displacement

The displacement at $x = 0$, (the *compliance*, or *approach*), is found from the shape integration by setting $x = 0$ ($\phi = \pi/2$). The results are shown in Fig. 6, where it is seen that the simple asymptote $R\delta = 0.5b^2(\ln(2.320\ d/b))$ is good up to $b/d \approx 0.2$. Above this, calculating the displacement due to a Hertzian pressure distribution $p = (E^*/2R)\sqrt{b^2 - x^2}$ is little better than simply using the asymptote. Examination shows that a pressure of the form $p = K\sqrt{1 - x^2/b^2}$ *can* give a reasonable answer, but only if the complete shape is calculated and the pressure then scaled to give the best fit to the indenter shape $z = x^2/2R$. In this way, good results are obtained up to $b/d = 1$: subsequently it seems $R\delta/b^2 \approx 0.6$ rather than the correct $R\delta/b^2 \to 0.5$ (Fig. 6).

It may be thought that the ordinate chosen, $R\delta/b^2$ is somewhat esoteric: why the interest in comparing indentations of the same width in layers of different thicknesses? The primary reason is indeed the authors' dislike of graphs with answers ranging over 10^4 as would the more natural $R\delta/d^2$. However, it may be noted

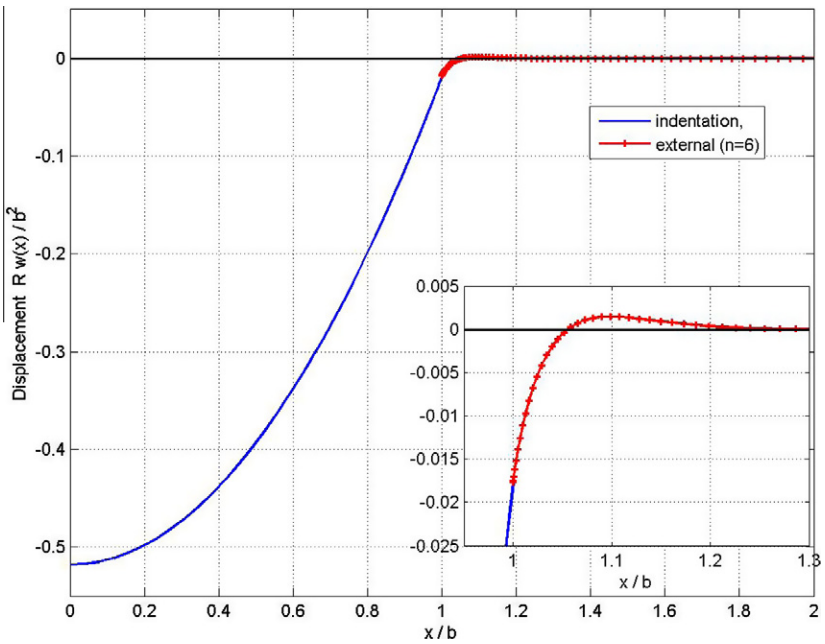

Fig. 7. Unbonded layer: shape outside contact region. The material displaced by the indenter is almost entirely accommodated by compression: the rise in the surface level outside the contact is almost negligible.

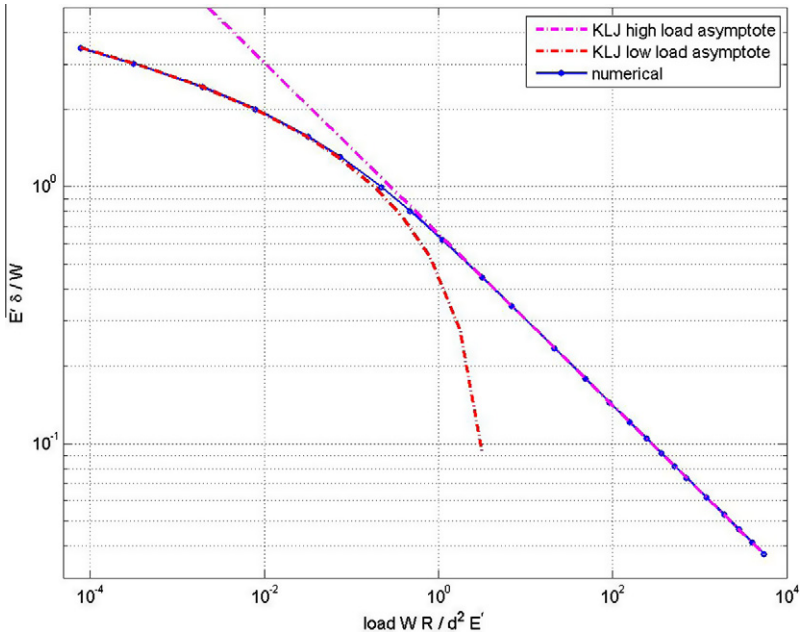

Fig. 8. Variation of displacement $E'\delta/W$ with load WR/d^2E'.

that if the edges $x = \pm b$ of the contact occurred at the height of the undeformed layer, then $\delta = b^2/2R$: if below this level, $\delta > b^2/2R$. Thus the parameter gives an indication of whether there is 'sinking-in' – as observed in a circular Hertzian contact, where $\delta = a^2/R$ – or 'piling-up', as can occur in a plastic indentation. For the unbonded slab, this never occurs: but see below for the bonded slab (Figs. 13 and 14). Note however that this refers only to piling-up *at* the contact edge: as Fig. 7 (for $\delta = 0.518b^2/R$) shows, the contact edge may lie below the original level while further away the surface may (very slightly) rise above that level.

The load is $W = b\int_{-1}^{1} p(t)dt = \frac{\pi b}{4}\left[c_0 - \frac{1}{2}c_1\right]$. Fig. 8 allows the variation with load of the more obvious parameter $R\delta/d^2$ to be found, although the ordinate is chosen to permit values to be read with some attempt at precision.

Approximations for the displacement for low and high load cases are given by Johnson (1985). The low load approximation $R\delta = 0.5b^2[\ln(2.320\ d/b)]$ (together with the Hertz equation $WR/E'b^2 = \pi/4$) is good for $WR/d^2E' < 0.1$, and is readily understandable. The high load approximation is $R\delta = 0.5b^2$, $WR/E' = (2/3)b^3/d$ leading to $R\delta/d^2 \sim (9/32)^{1/3}(WR/d^2E')^{2/3}$, and is excellent for

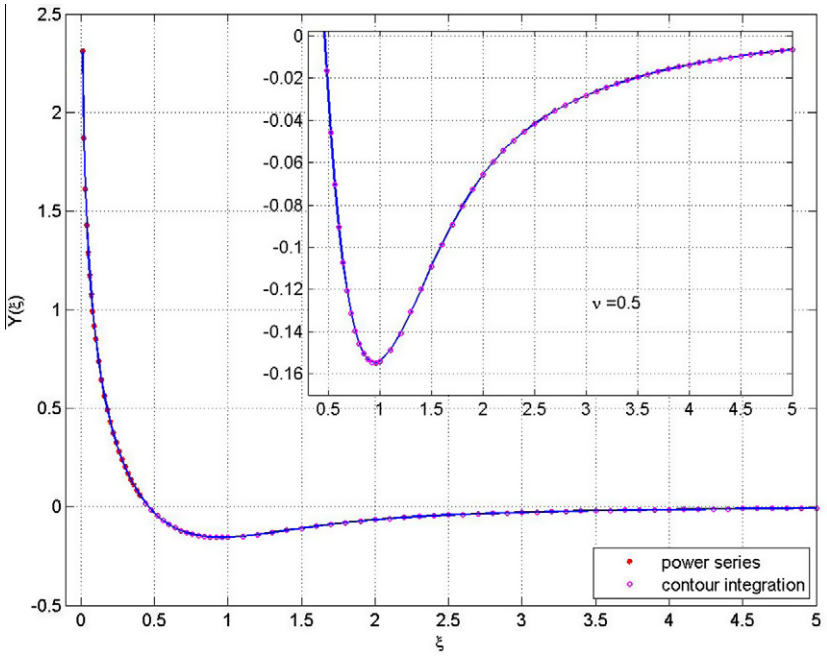

Fig. 9. Green's function for a bonded layer of incompressible solid. By using 40 poles contour integration can be used down to $\xi = 0.04$ (retaining 10^{-5} accuracy): by using 6 terms the power series may be used up to $\xi = 1$: clearly each has its useful range, but there is a very considerable overlap region.

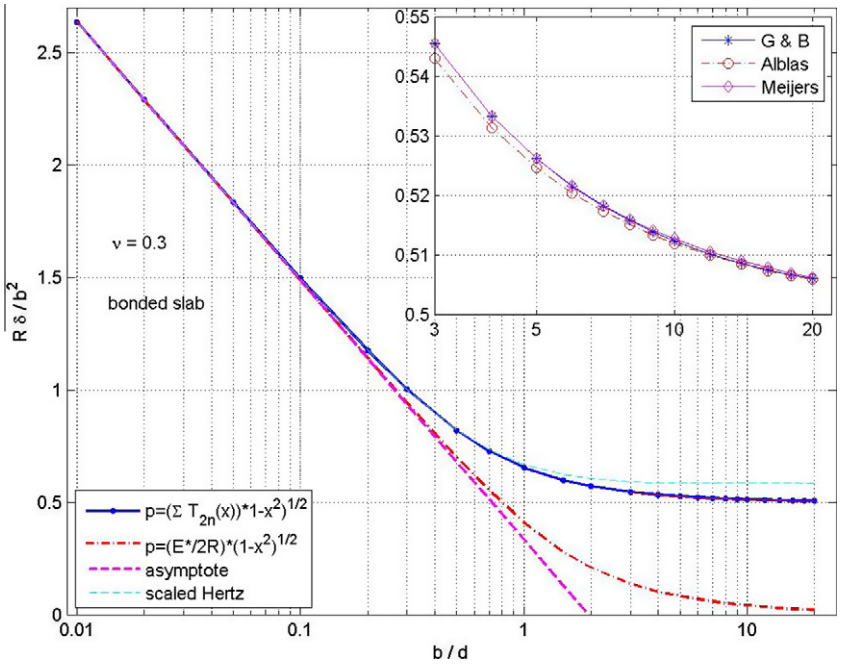

Fig. 10. Approach for low values of Poisson's ratio. $R\delta/b^2$ falls steadily to the asymptotic value 0.5, indicating that the contact edge is then at the undisturbed height.

$WR/d^2E' > 1$. This is somewhat surprising, for as Fig. 6 shows, $R\delta/b^2$ falls rather slowly to 0.5, and the pressure distribution is slow to attain the parabolic form assumed in the approximation.

4. Layer bonded to a rigid base

The more important case technologically is of an elastic layer bonded to a rigid base. This has been investigated in detail. (Hannah, Miller, Meijers) but in searching for a mathematically exact solution of the mixed boundary value problem (shape prescribed for $|x| < b$, zero pressure for $|x| > b$, difficult analysis has resulted. In particular, it seems that the case of the incompressible material $\nu = 1/2$ causes problems: indeed, even in Johnson's elementary analysis of the problem, the incompressible solid needs a separate analysis. By attempting to obtain only an approximate solution (but it seems probable, cf Fig. 4 above and many tests for the bonded layer, that the accuracy is high), none of these problems arise.

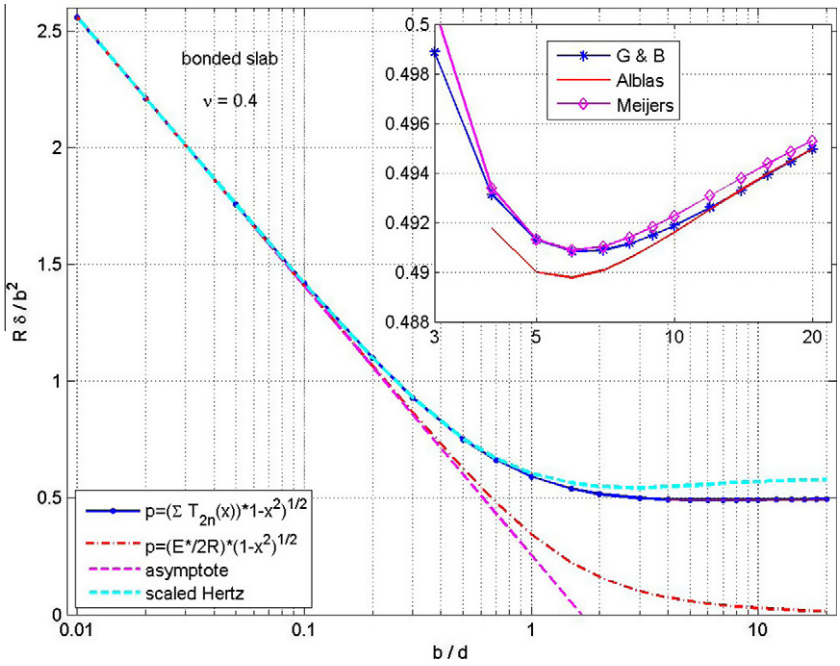

Fig. 11. Approach for $v = 0.4$ (Indenter shape fitted using 6 Chebyshev polynomials). A sign has been arbitrarily changed in the Alblas asymptote, see below.

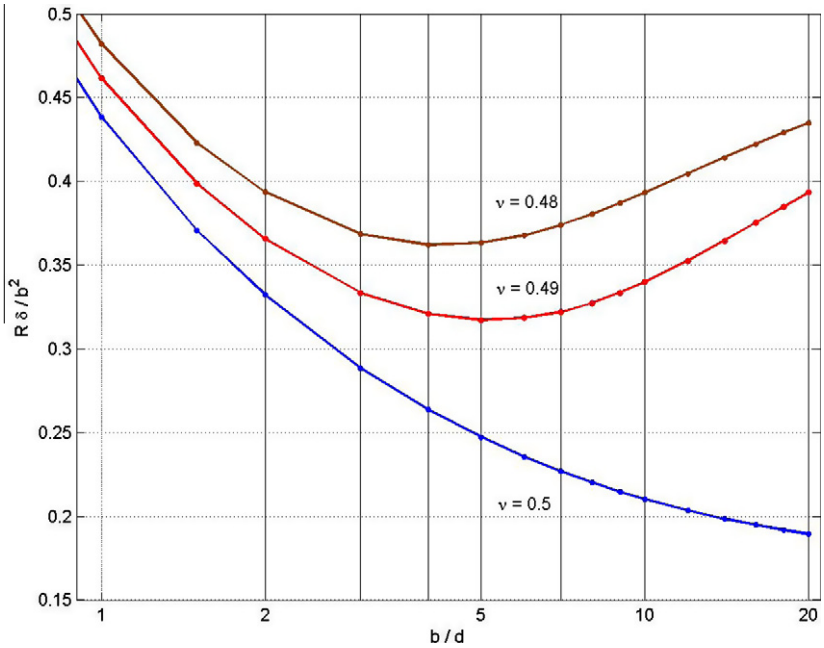

Fig. 12. Approach for incompressible and almost incompressible solids.

Hannah (1951) shows that the Green's function is now

$$Y(\xi) = \frac{2}{\pi}\int_0^\infty \frac{K_1\sinh(2\alpha) - 2\alpha}{K_1\cosh(2\alpha) + 2\alpha^2 + K_2}\cos(\alpha\xi)\frac{d\alpha}{\alpha}$$

where $K_1 = 3 - 4v$; $K_2 = K_1 + 2(1-2v)^2$.

The analysis follows exactly the same path as for the unbonded cylinder, with a solution for large ξ found by contour integration and a power series solution for small ξ. There is again a large range when the two solutions overlap and give the same results. The details are given in Appendix A.

The dominant term for $\xi > 1$ comes from the pole on the imaginary axis, so has no oscillatory component. The decay rate is $O(e^{-k\xi})$ with $k \approx 1$[2] compared with $O(e^{-2.1\xi})$ for the unbonded layer, so the significant range of the Green's function is much greater.

4.1. Indentation by a cylinder

The analysis now follows exactly the same procedure as for the unbonded layer. The results shown in Fig. 10 are typical for all $v \leqslant 0.3$: and resemble those for the unbonded layer.

For Poisson's ratio less than 0.3, the shape outside the indentation is very similar to that for the unbonded layer, with negligible

[2] $\exp(-k(v)\xi)$ with $k = 1.19, 1.09, 1.00, 0.91, 0.83, 0.74$ for $v = 0, 0.1, 0.2, 0.3, 0.4, 0.5$.

Table 2
Data for computing Green's function for the bonded layer.

(a) Bonded layer $0 \leqslant \xi \leqslant 0.4$
$Y(\xi) = -\frac{2}{\pi}\ln(\tanh(\pi\xi/8) + Y_b(\xi)$: $Y_b(\xi) = \sum_{n=0}^{5} b_n \xi^{2n}$

	n	0	1	2	3	4	5
$\nu = 0.3$	b_n	0.93032	−0.42308	0.15492	−0.05090	0.01563	−0.00460
$\nu = 0.4$	b_n	1.02985	−0.49437	0.18863	−0.06348	0.01974	−0.00584
$\nu = 0.49$	b_n	1.19194	−0.60268	0.24027	−0.08300	0.02616	−0.00780
$\nu = 0.5$	b_n	1.21667	−0.61892	0.24813	−0.08602	0.02716	−0.00810

(b) $\xi > 4 \quad Y(\xi) = -4\sum_{k=1}^{8} \exp(-\xi\, y_k)[A_k \cos(\xi\, x_k) + B_k \sin(\xi x_k)]$

Poles $z_k \equiv x_k + iy_k$		Residue factors $A_k + iB_k$[†]	
Bonded layer $\nu = 0.3$			
0.00000	0.91278i	0.00000	0.01285i
1.45379	2.57039i	−0.01768	−0.25010i
2.23310	5.91308i	0.00555	−0.08875i
2.64719	9.13968i	0.00440	−0.05561i
2.93600	12.33113i	0.00326	−0.04080i
3.15887	15.50616i	0.00249	−0.03231i
3.34065	18.67200i	0.00196	−0.02678i
3.49425	21.83210i	0.00159	−0.02289i
Bonded layer $\nu = 0.4$			
0.00000	0.82631i	0.00000	0.05108i
1.60943	2.53750i	0.00220	−0.24495i
2.36711	5.89487i	0.00784	−0.08842i
2.77705	9.12713i	0.00524	−0.05550i
3.06423	12.32154i	0.00370	−0.04075i
3.28629	15.49842i	0.00276	−0.03228i
3.46759	18.66550i	0.00215	−0.02676i
3.62089	21.82651i	0.00172	−0.02287i
Bonded layer $\nu = 0.49$			
0.00000	0.74790i	0.00000	0.12108i
1.78628	2.49302i	0.02314	−0.24021i
2.52422	5.87255i	0.01044	−0.08801i
2.93001	9.11200i	0.00622	−0.05536i
3.21555	12.31008i	0.00422	−0.04068i
3.43677	15.48918i	0.00308	−0.03224i
3.61758	18.65777i	0.00236	−0.02674i
3.77057	21.81986i	0.00188	−0.02285i
Bonded layer $\nu = 0.5$			
0.00000	0.73909i	0.00000	0.13193i
1.80936	2.48689i	0.02579	−0.23957i
2.54489	5.86956i	0.01077	−0.08795i
2.95017	9.10999i	0.00635	−0.05534i
3.23550	12.30856i	0.00428	−0.04067i
3.45661	15.48796i	0.00312	−0.03224i
3.63737	18.65675i	0.00239	−0.02673i
3.79031	21.81898i	0.00190	−0.02285i

[†] The residues are $(A_k + iB_k)\exp(i\xi z_k)$.

pile-up. However, Fig. 11 shows that for $\nu = 0.4$ a new feature occurs: instead of $R\delta/b^2$ decreasing steadily to 0.5, it overshoots before rising to the asymptotic value. An immediate reaction is that this is absurd, but comparison with asymptotes produced by Meijers (1968) and Alblas and Kuipers (1970) suggests that it is at least qualitatively correct.

The negative coefficient of $(d/b)^2$ given by Alblas for the asymptote (for *all* values of $\nu \leqslant 0.4$) gives implausibly low values when $\nu = 0.4$ for $b/d < 10$ (although the equation is said to be valid for all $b/d \geqslant 4$); and has arbitrarily been reversed for plotting Fig. 11 (see discussion): with this done, both asymptotes are close to the values found by the present method.

Results for larger values of ν repeat the pattern, with somewhat lower minimum values. Only for $\nu = 0.5$ is the behaviour different. As shown in Fig. 12, the incompressible solid follows the same pattern of the minimum of $R\delta/b^2$ steadily decreasing as ν increases, except that here the minimum may well be at infinity, with the value 1/6 as predicted by Meijers. For this case, numerical values

Table 3
Meijers and Alblas asymptotic results.

ν	$R\delta/b^2$ (Alblas)	$R\delta/b^2$ (Meijers (deduced))
U	$0.5 + 0.170(d/b) + 0.029(d/b)^2$	
0	$0.5 + 0.176(d/b) - 0.016(d/b)^2$ $d/b < 1$	$0.5 + 0.1831(d/b) + 0.0168(d/b)^2$
0.2	$0.5 + 0.173(d/b) - 0.001(d/b)^2$ $d/b < 1$	
0.3	$0.5 + 0.115(d/b) - 0.042(d/b)^2$ $d/b < 0.45$	$0.5 + 0.1221(d/b) + 0.0432(d/b)^2$
0.4	$0.5 - 0.118(d/b) - 0.340(d/b)^2$ $d/b < 0.25$	$0.5 - 0.1113(d/b) + 0.3395(d/b)^2$
0.45		$0.5 - 0.5487(d/b) + 1.2415(d/b)^2$
0.48		$0.5 - 1.5318(d/b) + 4.7117(d/b)^2$
0.5	$\frac{1+4.358(d/b)+0.9307(d/b)^2+0.098(d/b)^3}{6(1+1.4526(d/b)}$	$\frac{1+4.3772(d/b)+0.9868(d/b)^2+0.1041(d/b)^3}{6(1+1.4591(d/b)}$

U = Unbonded layer
In Meijers equations, terms $a_0\exp(-2A\, b/d)$ have been ignored since a_0 is not given.
For comparison, our results for ($\nu = 0.4$) are fitted by [0.5 −0.1198+0.3797] ($b/d = 4{:}20$).

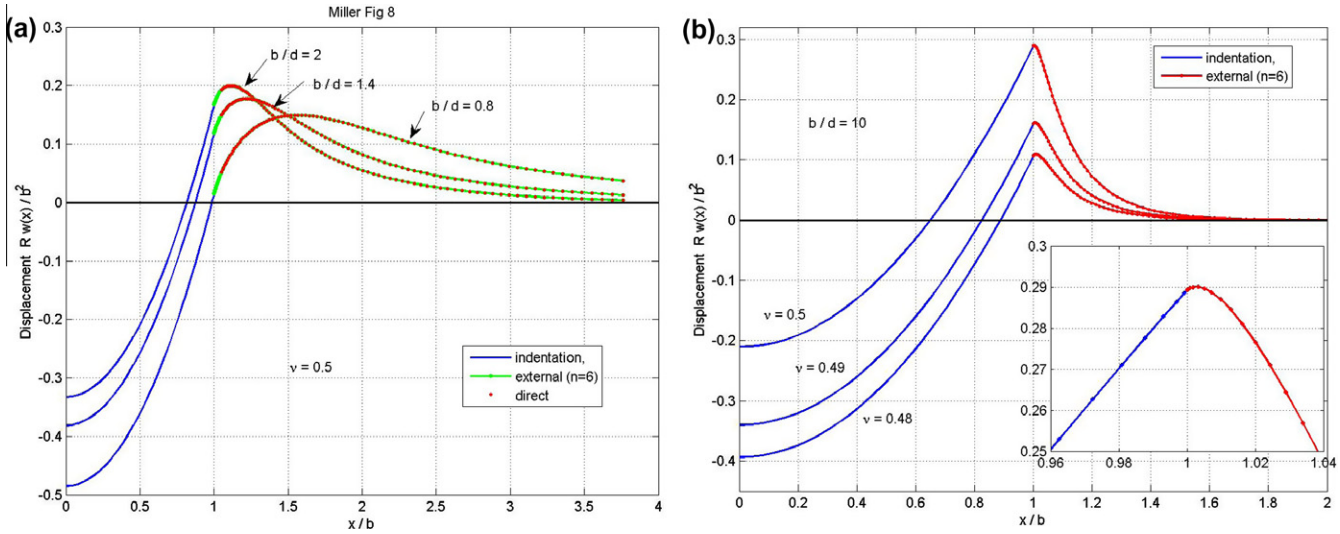

Fig. 13. (a) Bonded layer, as $\nu \to 0.5$. (b) Incompressible solid: results for moderate b/d. The curves are identical to those given by Miller (Fig. 8). The pile-up now accommodates all the volume of the indentation.

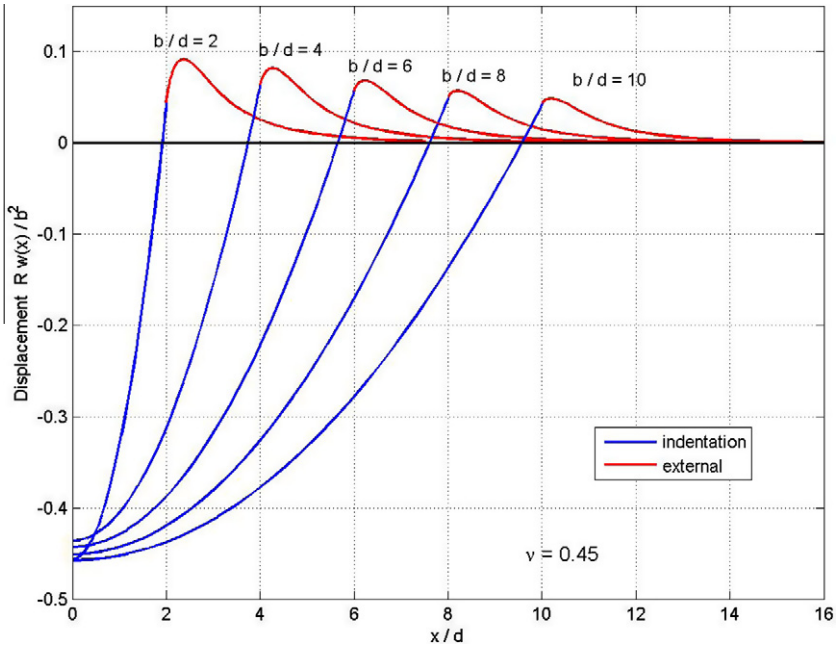

Fig. 14. Bonded layer showing effect of layer thickness.

from the Alblas & Kuiper asymptote are almost indistinguishable from those from Meijers' equation (see Table 3): and the agreement with our results appears to be perfect.

4.1.1. Asymptotic behaviour for small b/d

The linear decrease of $R\delta/b^2$ as $0.5\ln(d/b)$ is common to all values of ν (and for the unbonded layer); but the curves are not the same, being offset by an amount dependent on ν: so $R\delta/b^2 \sim 0.5\ln(d/b) + a(\nu)$. Values of $a(\nu)$ may be found from the values of b_0 given in Table 2 according to $a(\nu) = (1/4)[1 + 2\ln(16/\pi) - \pi b_0]$: but no simple equation for $a(\nu)$ or b_0 has been found. Argatov (2001) shows that $a(\nu) = 0.5(1 + ln(2)) + \int_0^\infty (1 - e^{-\alpha} - L(\alpha))d\alpha/\alpha$ where $L(\alpha) \equiv \frac{K_1 \sinh(2\alpha) - 2\alpha}{K_1 \cosh(2\alpha) + 2\alpha^2 + K_2}$ (or the corresponding function for the unbonded layer): values calculated from this integral are in excellent agreement with the values found here. An empirical fit (with a maximum error of 0.2% for $0 \leqslant \nu \leqslant 0.5$ is $a(\nu) \approx (0.41 - 0.5678\nu - 0.34\nu^2)/(1 - 1.24\nu)$. For comparison, the unbonded layer has $a = 0.5\ln(2.320) = 0.4208$.

4.1.2. Shape outside the indentation

The most convenient way to obtain the external shape is the direct numerical integration of the complete Green's function $Y(\xi)$ since this is negligible whenever ξ is large. However it is not easy to obtain accurate values when x/b is close to 1, so there the logarithmic term was again subtracted and integrated analytically (see Appendix C) and numerical integration performed on the reduced function $Y_m(\xi)$. Values of $R\delta/b^2$ approaching 1/2 suggest a rather different shape for the indentation from that shown in Fig. 7 for the unbonded layer. Fig. 13 shows examples of the behaviour, observed in less extreme form for values of Poisson's ratio exceeding

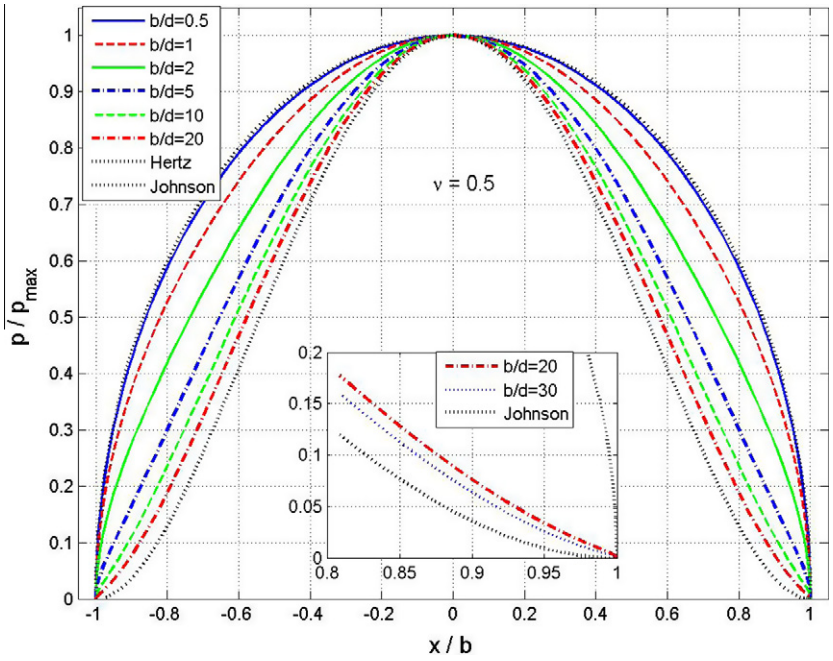

Fig. 15. Development of pressure distribution: bonded, incompressible layer.

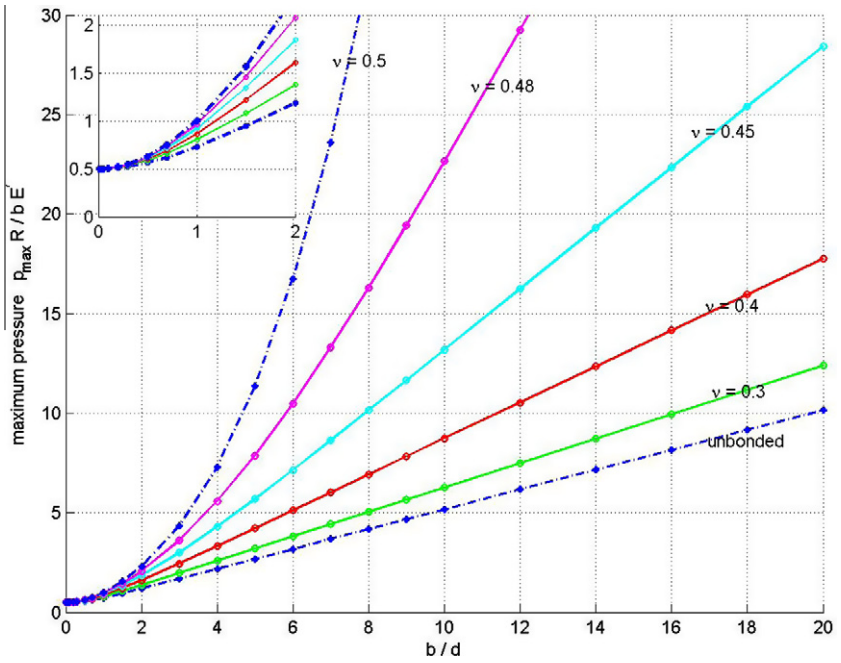

Fig. 16. Maximum pressure for unbonded and bonded layers. The slopes agree well with Johnson's asymptotic values.

perhaps 0.4. For the bonded, incompressible solid the volume of the pile-up must of course equal the volume of the indentation: the rather limited lateral extent guarantees the greater height. As Meijers points out, for large b/d when $R\delta/b^2 \sim 1/6$, the height of the pile-up will be twice the indentation depth.

As b/d increases, more and more of the displaced material is accommodated by compression, and the pile-up at the edge of the indentation decreases.

4.1.3. Pressure distributions

For moderate or small values of Poisson's ratio, the development of the pressure distribution as b/d increases is very much as for the unbonded layer Fig. 5, starting with the Hertzian distribution for $b/d \leqslant 0.5$ (initially with the Hertzian maximum pressure $p_0 = (E'b/2R)$ but then with the maximum increasing), and approaching Johnson's limiting parabolic distribution closely for $b/d \geqslant 10$.

In contrast, for the incompressible layer, a quasi-parabolic distribution is reached for $b/d \approx 5$ (Fig. 15), but the development continues, apparently approaching Johnson's second limit, $p \propto (1-x^2)^2$ at the limit of our calculations. (Our arbitrary limit of 6 terms of the pressure series restricted us to b/d up to 30).

The maximum pressures agreed well with Johnson's linear asymptote $Rp_{\max}/bE' \sim C(\nu)\cdot(b/d)$ with $C(\nu) = (1-\nu)^2/(2(1-2\nu))$ for $\nu \leqslant 0.45$ but with an offset (see Fig. 16), and qualitatively with

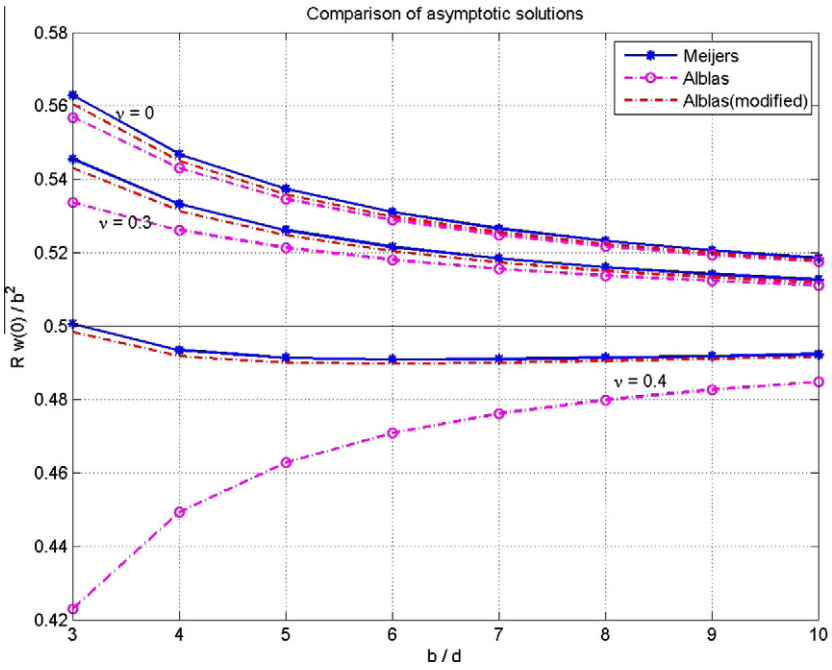

Fig. 17. Comparison of Meijers and Alblas asymptotes. Changing the signs of the Alblas quadratic coefficients results in good agreement between the two.

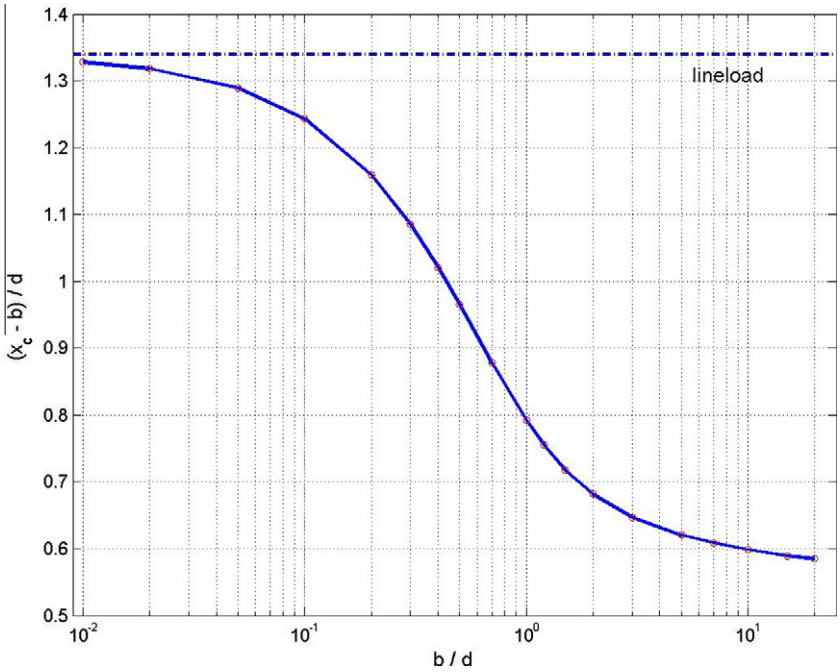

Fig. 18. Location at which interface pressure becomes negative.

his result for $\nu = 0.5$ $[Rp_{\max}/bE' \sim (1/24)\cdot(b/d)^3]$. For $0.45 < \nu < 0.5$ the initial curvature persisted to higher values of b/d, and it was not possible to determine a slope.

5. Discussion: asymptotes and accuracy

For the incompressible solid ($\nu = 0.5$), Meijers and Alblas give almost identical asymptotes, and the agreement between these and the present results appears perfect. This confirms the accuracy of our numerical procedure: and since it applies without any noticeable changes to all values of Poisson's ratio, suggests to us that all our results are trustworthy.

In contrast, while the analyses by Meijers and Alblas each lead to a simple quadratic in (d/b) (instead of a rational function as found for $\nu = 0.5$), the two asymptotes have a glaring difference in the sign of the coefficient of $(d/b)^2$: Alblas throughout giving negative values, Meijers positive values. Of the cases given by both authors, the quadratic coefficients are small and the resulting differences in $R\delta/b^2$ are unimportant except for $\nu = 0.4$, for which Alblas gives

$$\frac{R\delta}{b^2} \sim 0.5 - 0.118(d/b) - 0.349(d/b)^2 \quad (\nu = 0.4)$$

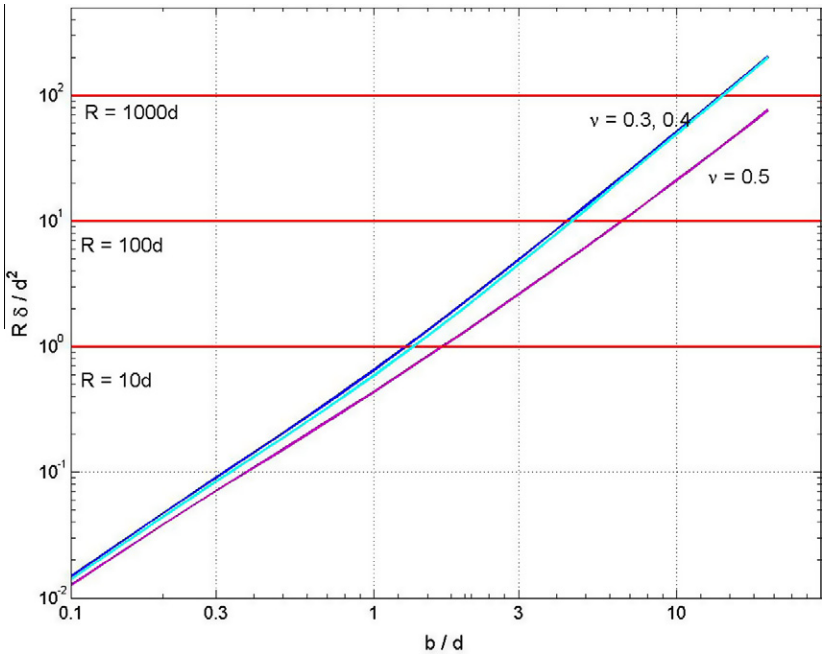

Fig. 19. Restrictions on indenter radius.

while Meijers' answer, extracted with some difficulty from his data,[3] is

$$\frac{R\delta}{b^2} \sim 0.5 - 0.1113(d/b) + 0.3395(d/b)^2 \quad (\nu = 0.4)$$

Neither author actually plots the quantity $R\delta/b^2$, preferring instead the more obvious variable $R\delta/d^2$: and this of course tends peaceably to zero as $d/b \to \infty$, so the implausible behaviour of the Alblas equation for $\nu = 0.4$ (Fig. 17) is not apparent. The experiment of altering the sign was tried, with such success that the remaining signs were also changed. This results in curves always close to the Meijers curves, and, as shown in Fig. 11, to values in good agreement with those found by our analysis.

We note that the Meijers and Alblas analyses (and the elementary analysis of the limiting behaviour provided by Johnson) treat the incompressible solid as a completely separate case, so the accuracy of the result for $\nu = 1/2$ does not imply that the results for $\nu < 1/2$ are accurate.

The "corrected" Alblas curves agree with our results better than do the Meijers curves. The sign error, if it exists, is certainly not a misprint, as it follows earlier stages of the analysis and is adopted in Alblas' Fig. 2: but it seems not impossible that at some point in an analysis involving $S_+(0), iS'_+(0), S''_+(0), S_-(0), iS'_-(0), S''_-(0)$ a factor i^2 might have been omitted.

There would seem to be a strong case for yet a third formal analysis of the asymptotic behaviour for large (b/d).

5.1. Choice of method

It seemed convenient to us to obtain accurate numerical values of the Green's function for indentation of a layer, and use this to find the deformation due to a chosen pressure distribution. Initially the form of this was a polynomial multiplying the $\sqrt{1-x^2/b^2}$ factor, but it became apparent that the polynomial was better replaced by the equivalent Chebyshev series to give $p(x) = \sqrt{1-x^2/b^2}\sum c_n T_{2n}(x/b)$. This brings our method closer to that devised by Gladwell (1976) and followed by Jaffar and Savage (1988) and Jaffar (1993), except that they multiplied their series by the singular factor $1/\sqrt{1-x^2/b^2}$. But the condition that the pressure vanishes at $x = b$ guarantees that the *sum* of the series has a factor $(1 - x^2/b^2)$, so it seems preferable to use this information from the outset and avoid individual singular terms. We also find it unnecessary to follow them in choosing the load as the independent variable and so converting their solution of the integral equation into an eigenvalue problem: the contact width parameter b/d seems completely satisfactory. But the major difference is that we devote the major effort to the accurate determination of the Green's function. Gladwell subtracts from the integrand of the Green's function a term which can be integrated analytically: he then integrates the balance by expanding it in a series valid for $x/b < 1$ and using a sophisticated method of summing it for all x/b. Jaffar & Savage appear not to find the whole Green's function explicity, but to leave the balance to be found within the final double numerical integration. All may be well: but it is difficult to explain why Jaffar & Savage found it necessary to use over 20 terms of the pressure series for $b/d = 5$ to obtain their desired accuracy while we use at most six: nonetheless, to pick a value quoted specifically by Jaffar (1993), our value for $b/d = 10$, $\nu = 0.3$ agrees well with the Meijers and Alblas asymptotes (0.512–0.513) in contrast to Jaffar's 0.505. (Recall that it is the difference from the limiting value 0.5 which is relevant).

5.2. Inapplicability

(1) Layer 'resting' on a rigid base.

Filon (1903) discovered that when a line load is applied to an elastic layer resting on a rigid base, contact between the layer and the base is lost at a distance of approximately $\pm 1.35d$ from the load. (The phenomenon was rediscovered in the 1970s, and named, with a splendid disregard for the English language since it occurs immediately and completely, a "receding contact"). The interface pressures are readily found once the surface pressures are known, and again reveal tensile pressures at a distance of the order of the layer thickness beyond the contact edge, as shown in Fig. 18.

[3] And ignoring terms multiplied by a factor exp(-1.4b/d).

Clearly this is no problem if the elastic layer is really attached to the rigid base, but if it is, as is more natural, simply resting on the base, the analysis is no longer applicable. One can only hope that the resulting redistribution of the stresses has a negligible effect.

(2) Restriction on indenter radius.

If the indentation depth becomes a serious fraction of the layer depth, [$\delta = 0.1d$ to give strains of 10%?] the use of linear elasticity becomes highly suspect. [Even more restrictive is the need to avoid plastic yield]. Taking this very tolerant limit of $\delta = 0.1d$, we must have $R\delta/d^2 < 0.1(R/d)$. Fig. 19 shows the implications for bonded slabs. Results are valid only below the horizontal (red) lines. Thus, only for an indenter radius a thousand times the layer thickness can the results be believed up to $b/d \approx 15$: for $R = 10d$ the limit is $b/d \approx 1.5$ (slightly higher for $\nu = 0.5$). The modifications for a more realistic limit of $p_{max} < 0.01E$ will be obvious.

5.3. Application to axial symmetry?

The similarity between the plane strain and the axially symmetric problems is well-known.

For the surface deflection of an unbonded layer under an axially symmetric pressure distribution Sneddon (1946)[4] gives

$$u(r) = \frac{4}{E'}\int_0^\infty \bar{p}(\xi)\frac{\sinh^2(\xi d)}{\sinh(2\xi d)+2\xi d}J_0(\xi r)d\xi$$

$$\text{where } \bar{p}(\xi) = \int_0^\infty rp(r)J_0\xi r)dr$$

and comments that this and his other " integral expressions... are exactly similar to the 'Fourier' integrals obtained by Filon (1903) in his solution of the two-dimensional analogue of this problem". Dougall (1904) shows that this may be evaluated by a contour integration of $\int \bar{p}(z)\frac{\sinh^2(zd)}{\sinh(2zd)+2zd}H_0^{(2)}(zr)dz$ (the terminology and notation for Bessel functions has changed since 1904). But to use our method, the next step is to find the deflection due to a ring load. Formally this is no problem: a ring load at $r = c$ of magnitude p_1 per unit distance gives $\bar{p}(\xi) = p_1 cJ_0(\xi c)$: the poles are again the zeros of $\sinh(2zd) + 2zd$ and the residues could be extracted by MATLAB as before. The drawback is that instead of a single Green's function $Y(x/d)$, we need a separate Green's function for each individual ring load: a function $Y(r/d, c/d)$. We can only say that this would be a ponderous method.

6. Conclusions

An efficient and accurate method has been developed for finding the Green's function for the indentation of an elastic layer resting on or bonded to a rigid base. From the form of the equations it is clear that the function is oscillatory when the layer is free to slip over the base, but for the bonded layer, the function simply decays to zero after a single overshoot.

By calculating the deformation due to pressure distributions of the form of the product of a polynomial with a elliptical ("Hertzian") term and choosing the coefficients suitably, the indentation shape can match the shape of a cylindrical indenter to high accuracy. The resulting pressure distributions behave much as in Johnson's approximate theory, becoming parabolic instead of elliptical as the ratio b/d of contact width to layer thickness increases, or, for the *bonded incompressible* ($\nu = 1/2$) layer, becoming bell-shaped for very large b/d.

[4] But beware of Sneddon's numerical results, with their remarkable feature that on the axis $r = 0$, $\sigma_r \neq \sigma_\theta$! see (Greenwood, 1964) for details.

The relation between the approach δ and the contact width b (in the form of $R\delta/b^2$: b/d curves has been investigated, and some anomalies in published asymptotic equations noted and, perhaps, resolved. A noticeable feature of our method is that, unlike previous solutions in which the full mixed boundary value problem (given indenter shape: stress-free boundary) has been solved, the bonded incompressible solid causes no problems and is handled just as for lower values of Poisson's ratio. Despite this similarity of the analysis, the known distinction between $R\delta/b^2 \to 1/2$ as $b/d \to \infty$ for all $\nu < 1/2$ and $R\delta/b^2 \to 1/6$ for $\nu = 1/2$ is again found.

It is noted that Filon's phenomenon of lift-off will invalidate the analysis for the unbonded layer *resting* on a rigid base and so unable to provide the tensile stresses required for contact: but the necessary tensile stresses are so small that it seems unlikely that the stress redistribution will cause a detectable change in any of the results. A more serious restriction on the applicability of the theory is that large values of b/d can be achieved *within the elastic limit* only when the indenter radius is large compared to the thickness of the layer.

Appendix A. Green's function for a layer bonded to a rigid base

Hannah (1951) shows that the Green's function is now

$$Y(\xi) = \frac{2}{\pi}\int_0^\infty \frac{K_1\sinh(2\alpha) - 2\alpha}{K_1\cosh(2\alpha) + 2\alpha^2 + K_2}\cos(\alpha\xi/d)\frac{d\alpha}{\alpha}$$

where $K_1 = 3 - 4\nu$; $K_2 = K_1 + 2(1 - 2\nu)^2$.

The function $F(z) \equiv \frac{K_1\sinh(2z)-2z}{K_1\cosh(2z)+2z^2+K_2}$ is bounded on the circle $z = (2k + 0.5)\pi\exp(i\theta)$ in the upper half plane [maximum $\approx 1 + C(\nu)\exp(-0.7113k)$ with $C(\nu) = O(10^{-4})$ so max $\approx 1 + 10^{-7}$ for all values of ν].

Hence the integrand $\{F(z)/z\}\exp(i\xi z)$ again satisfies the conditions of Jordan's lemma, and the integral along the real axis is equal to $2\pi i$ times the sum of the residues in the upper half plane.

The only poles in the upper half plane are at the zeros of $K_1\cosh(2z) + 2z^2 + K_2$ ($z = 0$ is again not a pole as the numerator of $F(z)$ vanishes there); these are readily found much as before. Fig. A1 shows that they follow the same pattern as the poles of the unbonded layer, except that now there is also a single pole on the imaginary axis. Again, the case $\nu = 0.5$ seems in no way special, either in the location of the poles, or in the residues there.

[The pole on the imaginary axis gives rise to a simple exponential decay, and as this is the dominant term, the Green's function is not oscillatory.]

A.1. Combination of residues in the first and second quadrants

Near a pole z_k, the denominator $D(z) \equiv z[K_1\cosh(2z) + 2z^2 + K_2]$ of $\frac{K_1\sinh(2z) - 2z}{z[K_1\cosh(2z) + 2z^2 + K_2]}$ is approximately $D(z_k + t) \sim t\{z_k[2K_1 \sinh(2z_k) + 4z_k]\}$ so the residue is $\frac{K_1\sinh(2z_k) - 2z_k}{2z_k[K_1\sinh(2z_k) + 2z_k]} = \frac{1}{2z_k} - \frac{2}{[K_1\sinh(2z_k) + 2z_k]} \equiv A_k + iB_k$.

At the image pole $z = -x_k + iy_k = conj(-z_k) = -\bar{z}_k$ the residue will be $-\frac{1}{2}\left[\frac{1}{\bar{z}_k} - \frac{4}{[K_1\sinh(2\bar{z}_k) + 2\bar{z}_k]}\right] = -[A_k - iB_k]$, and these combine just as for the unbonded layer (but note there is also the contribution from the single pole on the imaginary axis).

Once again, the number of residues needed increases as $\xi \to 0$ (approximately as $1/\xi$), so it is convenient to obtain a power series to obtain the answers for small ξ. The Green's function is again decomposed into a term which can be integrated analytically and a correction term $Y_{2b}(\xi)$:

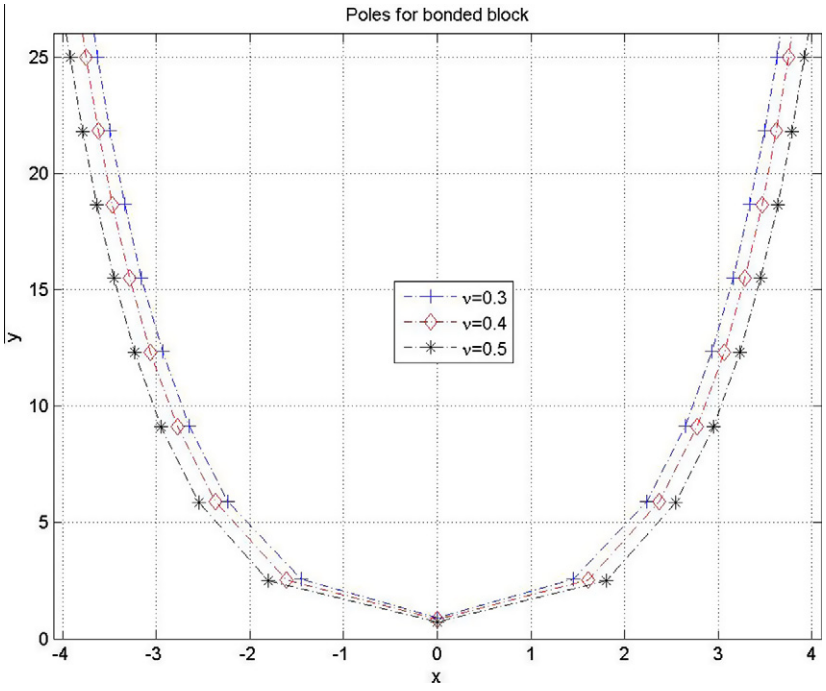

Fig. A1. Poles for integrand for layer bonded to rigid base. The poles for the incompressible solid ($\nu = 1/2$) do not appear to be special.

$$Y_b(\xi) = \frac{2}{\pi}\int_0^\infty \tanh(2\alpha)\cos(\alpha\xi/d)\frac{d\alpha}{\alpha} - Y_{2b}(\xi)$$

where

$$Y_{2b}(\xi) = \frac{2}{\pi}\int_0^\infty \frac{2\alpha\cosh(2\alpha) + (K_2+2\alpha^2)\sinh(2\alpha)}{\cosh(2\alpha)[K_1\cosh(2\alpha)+2\alpha^2+K_2]}\cos(\alpha\xi)\frac{d\alpha}{\alpha}$$

$Y_{2b}(\xi)$ is found by expanding the cosine in series and integrating term-by-term, while the first term is $-\frac{2}{\pi}ln\{\tanh(\pi\xi/8)\}$.

Appendix B. Virtue of Chebyshev expansion

For $\nu = 0.5$, $b/d = 10$ the coefficients c_n in the Chebyshev expansion of the series modifying the Hertz term are $(c_0, c_1 \ldots c_n)$

$$p(\cos\theta) = \sin\theta\sum c_n\cos 2n\theta$$

$$c_n = [29.36501\ -24.32090\ 1.26059\ 0.05840\ 0.03364\ 0.01432].$$

and one can believe that higher terms do not matter.

The power law version of this is

$$p(x) = \sqrt{1-x^2}\sum A_n x^{2n}$$

$$A_n = [54.9074\ -58.0357\ 6.9354\ 9.2960\ -14.0239\ 7.3318]$$

and now it is far from clear that the next term (x^{12}) may be neglected.

We note an incidental virtue of the Chebyshev form: the load is $b\int_0^\pi \sum c_n \sin^2\theta\cos(2n\theta)d\theta = \frac{\pi}{2}b[c_0 - \frac{1}{2}c_1]$;

the remaining terms contributing nothing.

Appendix C. Numerical integration of the logarithmic term

$$E'w_s(x) \equiv \frac{2b}{\pi}\int_{-1}^{+1} p(t)\ln\{|x-t|(b/d)\}dt$$
$$= \frac{4b}{\pi}\int_0^{+1} p(t)\ln\{b/d\}dt + \frac{2b}{\pi}\int_0^{+1} p(t)\ln\{|x^2-t^2|\}dt$$

since the pressure $p(t)$ is symmetric.

Setting $t = \cos\theta$ and using a Chebyshev expansion to describe the pressure

$$p(\cos\theta) = \sqrt{1-t'^2}\sum c_n T_{2n}(t') = \sin\theta\sum c_n\cos 2n\theta$$

gives

$$E'w(x)/b = \left(c_0 - \frac{1}{2}c_1\right)\ln(b/d) + \frac{2}{\pi}\sum c_n\int_0^{+\pi/2}\sin^2\theta\cos(2n\theta) \times \ln\{|x^2-\cos^2\theta|\}d\theta$$

and the second term is

$\frac{1}{2\pi}\sum c_n\int_0^{\pi/2}[2\cos 2n\theta - \cos(2n+2)\theta - \cos(2n-2)\theta]\ln\{|x^2-\cos^2\theta|\}$ so we need consider only the simpler integrals $I_{2n}(x) \equiv \int_0^{+\pi/2}\cos(2n\theta)\ln\{|x^2-\cos^2\theta|\}d\theta$.

For $|x| \leqslant 1$, we set $x = \cos\phi$ and write

$x^2 - \cos^2\theta = (1/2)(\cos 2\phi - \cos 2\theta)$

$$I_{2n}(x) = -\ln 2\int_0^{\pi/2}\cos(2n\theta)d\theta + \int_0^{\pi/2}\cos(2n\theta)\ln\{|\cos 2\phi - \cos 2\theta|\}d\theta$$

and the last is a known integral:

$$\int_0^{\pi/2}\cos 2n\theta\ln\{|\cos 2\phi - \cos 2\theta|\}d\theta = \begin{bmatrix} -(\pi/2n)\cos 2n\phi & \text{for } n>0 \\ -(\pi/2)\ln 2 & \text{for } n=0 \end{bmatrix}$$

while the first vanishes for $n = 1,2,3\ldots$ and equals $-(\pi/2)\ln 2$ for $n = 0$.

Hence we get the shape as a sum of $\cos(2n\phi)$ terms which are readily converted into a power series in t^{2m}.

For $|x| \geqslant 1$, we set $x = \cosh\alpha$ and obtain $I_{2n}(x) \equiv -\ln 2\int_0^{+\pi/2}\cos(2n\theta)d\theta + \int_0^{+\pi/2}\cos(2n\theta)\ln(|\cosh 2\alpha - \cos 2\theta|)d\theta$ and the last may be shown to equal $-(\pi/2n)\exp(-2n\alpha)$ for $n = 1,2,3\ldots$, but $-\pi\ln(2) + 2\alpha$ for $n = 0$. [We note that for $x = 1$ the two equations agree].

Appendix D. Alblas and Meijers asymptotes for large b/d

Alblas & Kuiper give a table of coefficients for their equations $R\delta/b^2 \sim 0.5 + a_1(d/b) + a_2(d/b)^2$ for $\nu = 0, 0.2, 0.3, 0.4$.

Meijers gives data from which equations of this form may be derived, for $\nu = 0, 0.3, 0.4, 0.45, 0.48$.

Three points should be noted.

(1) Alblas & Kuiper give a figure showing their asymptotes, corresponding to the published signs: the error, if it is an error, is not a simple misprint.
(2) The coefficients are obtained by 'analytical' methods, so should in principle be exact, and so identical. This is not the case: they are only 'reasonably' close.
(3) The asymptotes for the incompressible solid ($\nu = 0.5$) are not found by the same method as those for $\nu < 0.5$, and have a different form (the quotient of a cubic and a linear factor). The results agree with no tampering with the signs.

References

Alblas, J.B., Kuipers, M., 1970. On the two-dimensional problem of a cylindrical stamp pressed into a thin elastic layer. Acta Mech. 9, 292–311.
Aleksandrov, V.M., 1969. Asymptotic solution of the contact problem for a thin layer. PMM 33, 49–63.
Argatov, I.I., 2001. Solution of the plane Hertz problem. J. Appl. Math. Tech. Phys. 42, 1064–1072.
Dougall, J., 1904. The equilibrium of an isotropic elastic plate. Trans. Roy. Soc. Edinburgh 41, 129–228.
Filon, L.N.G., 1903. On the approximate solution for the bending of a beam of rectangular cross-section. Phil. Trans. A201, 63–155.
Gladwell, G.M.L., 1976. Some unbounded problems in plane elasticity theory. J Appl. Mech. (ASME) 43, 263–267.
Greenwood, J.A., 1964. The elastic stresses produced in the mid-plane of a slab by pressures applied symmetrically at its surface. Proc. Camb. Phil. Soc. 60, 159–169.
Hannah, M., 1951. Contact stress and deformation in a thin elastic layer. Quart. J. Mech. Appl. Math. 4, 94–105.
Jaffar, M.J., 1993. Determination of surface deformation of a bonded elastic layer indented by a rigid cylinder using the Chebyshev series method. Wear 170, 291–294.
Jaffar, M.J., Savage, M.D., 1988. On the numerical solution of line contact problems involving bonded and unbonded strips. J. Strain Anal. 23, 67–77.
Johnson, K.L., 1985. Contact mechanics. CUP.
Meijers, P., 1968. The contact problem of a rigid cylinder on an elastic layer. Appl. Sci. Res. 18, 353–383.
Miller, R.D.W., 1966. Some effects of compressibility on the indentation of a thin elastic layer by a smooth rigid cylinder. Appl. Sci. Res. 16, 405–424.
Sneddon, I.N., 1946. The elastic stresses produced in a thick plate by the application of pressure to its free surface. Proc. Camb. Phil. Soc., 260–271.